JAM CM Journal of Applied Mathematics and Computational Mechanics 2020, 19(2), 43-57
www.amcm.pcz.pl p-ISSN 2299-9965
DOI: 10.17512/jamcm.2020.2.04 e-ISSN 2353-0588

INFLUENCE OF THERMAL DIFFUSION ON MHD RADIATING FLOW IN PRESENCE OF *Cu*-NANOPARTICLES, CASSON FLUID AND ANGLE OF INCLINATION

***S. Brahma Chary*[1], *K. Jayarami Reddy*[2], *K. Kashaiah*[3]**

[1] *Research Scholar, KLEF, Guntur, Andhra Pradesh State, India*
[1] *Department of Mathematics, Sreenidhi Institute of Science and Technology Hyderabad, Telangana State, India*
[2] *Department of Mathematics, KLEF, Guntur, Andhra Pradesh State, India*
[3] *Department of Mathematics, Bharath Institute of Engineering and Technology Hyderabad, Telangana State, India*
chary442@gmail.com

Received: 5 November 2019; Accepted: 7 May 2020

Abstract. In this study numerical solutions for magnetohydrodynamic transfer, thermal and mass instability, free convection flow through the plate before Casson fluid, heat dissipation, thermal radiation, heat sink, chemical reaction, tilt angle, and saturated porous medium were described. The effectiveness of this study is to analyze the effect of heat diffusion, Casson fluid, the angle of interest on the flow phenomenon of *Cu*-nanoparticles in the presence of thermal radiation, heat source/heat sink, destructive reaction, heat transfer and mass transfer in a simple way. The finite difference method was used to solve the governing equations which are the added partial differential equations. The effects of different material parameters on velocity, temperature and concentration profiles are explained using graphs and tables. The results are compared with previously published papers and a very good agreement is found. In the boundary layer region, fluid velocity decreases with the increasing values of magnetic field parameter, heat source/sink, Casson fluid, angle of inclination and thermal radiation parameter for *Cu*-nanoparticles. Also it is noticed that the solutal boundary layer thickness decreases with an increase in the chemical reaction parameter. It is because chemical molecular diffusivity reduces for higher values of *Kr*.

MSC 2010: *76W05, 76S05, 65M06, 76D05*
Keywords: *thermal diffusion, Cu-nanoparticles, MHD, thermal radiation, Casson fluid*

1. Introduction

Nanofluids means the addition of nanoparticles to conventional working fluids that are containing a liquid of nanometer-sized particles that can improve heat transfer and solar energy collection. Recently, nanofluids attracts a great deal of interest with their enormous potential to provide enhanced performance properties,

particularly with respect to heat transfer. Nanoparticles in the base fluid (nanofluid) provide the following possible advantages in the solar energy absorption system: (i). Nanofluids can absorb energy with a directly-skipping intermediate heat transfer step, (ii). Nanofluids can be optically selective (i.e., high absorption in the solar range and low emittance in the infrared), (iv). Absorption efficiency may be enhanced by tuning the nanoparticle size and shape regarding or the proposed application [1]. Due to the bright future which is predicted for nanofluids, several studies of convective heat transfer in nanofluids have been conducted recently. Hayat et al. [2] studied flow with a heat transfer of nanofluid with mixed convection and non-linear thermal radiation effects in an inclined stretching sheet. The stagnation point flow of nanofluid with a melting heat transfer is analyzed by Hayat et al. [3]. They considered the heat generation/absorption effect as well as new condition of mass flux. Akdag et al. [4] numerically studied the heat transfer characteristics of Al_2O_3-water based nanofluids in a wavy mini-channel under pulsating inlet flow conditions. Hayat et al. [5] investigated the problem of MHD Falkner-Skan flow of a second grade nanofluid in a stretching wedge with melting heat transfer and heat generation/absorption effects. Pattnaik et al. [6] studied radiation and mass transfer effects on MHD flow through a porous medium past an exponentially accelerated inclined plate with variable temperature. Krishna Prasad et al. [7] studied double diffusive effects on mixed convection casson fluid flow past a wavy inclined plate in the presence of a darcian porous medium. Srinivasa Raju et al. [8] studied Jeffrey fluid impact on magnetohydrodynamic free convective flow past a vertically inclined plate with transfer effects through EFGM solutions. Sarada et al. [9] studied heat and mass transfer effects on chemical reacting fluid flow past an exponentially accelerated vertical plate. Jitthender Reddy et al. [10] studied the influence of viscous dissipation on unsteady MHD natural convective flow of casson fluid over an oscillating vertical plate via the finite element method. Srinivasa Raju [11] studied unsteady MHD boundary layer flow of Casson fluid over an inclined surface embedded in a porous medium with thermal radiation and chemical reaction. Rafique et al. [12] studied the brownian motion and thermophoretic diffusion effects on Micropolar type nanofluid flow with soret and dufour impacts over an inclined sheet using Keller-Box solutions. Rafique et al. [13] found the numerical solutions of Casson nanofluid flow over a nonlinear inclined surface with soret and dufour effects by the Keller-box method. Rafique et al. [14] discussed the Keller-Box analysis of the Buongiorno model with brownian and thermophoretic diffusion for casson nanofluid over an inclined surface. Rafique et al. [15] studied numerical analysis with the Keller-Box scheme for a stagnation point effect on flow of micropolar nanofluid over an inclined surface. Anwar et al. [16] studied numerical study of hydrodynamic flow of a Casson nanomaterial past an inclined sheet under a porous medium.

The novelty of the present study is the numerical investigate the effects of pertinent physical parameters on velocity, temperature and concentration distributions for non-newtonian nanofluid in the presence of Casson fluid, *Cu*-nanoparticles, chemical reaction, thermal radiation, heat source/sink, transverse magnetic field,

thermal diffusion, heat and mass transfer towards a vertically inclined plate. In the present study, we extend the work of Pattnaik et al. [6] by considering nanofluid namely, Casson fluid and thermal diffusion effects. The problem of MHD unsteady flow of a Cu-nanoparticles with heat and mass transfer through a non-Darcy porous medium towards a vertically inclined vertical plate in the presence of thermal diffusion and Casson fluid is studied. Effects of free convection, in the presence of thermal radiation, heat source/sink, chemical reaction is taken into our consideration. Solutions for the momentum, energy and species diffusion equations are obtained by using Finite difference method (FDM). Numerical results for the velocity, temperature and concentration distributions are obtained.

2. Flow governing equations

In this problem, we studied the aspects of an unsteady heat and mass transfer, MHD free convective flow of radiating and chemically reacting fluid flow past an exponentially accelerated inclined infinite plate with variable temperature embedded in a saturated porous medium in the presence of *Cu*-nanoparticles and heat source/sink. The physical model is represented in Figure 1. For this investigation, the following assumptions are made:

i. The x'-axis is taken along the plate and y'-axis is normal to the plate.
ii. Magnetic field of intensity B_0 is applied in the direction perpendicular to the plate.
iii. At the beginning, it meant that at the time $t' \leq 0$, the fluid towards a stationary plate is kept at a uniform temperature T'_∞, the concentration of the species on the surface of the plate and at each point in the fluid kept at a uniform concentration C'_∞.
iv. Also, at $t' > 0$, the temperature at the surface of the plate is raised to uniform temperature T'_w and species concentration at the surface of the plate is raised to uniform species concentration C'_w and is maintained thereafter.
v. The plate is inclined to a vertical direction by an angle α.
vi. The induced magnetic field is neglected as the magnetic Reynolds number of the flow is very small.
vii. It is believed that the induced magnetic field produced by the motion of the fluid is negligible compared to the applied field. This assumption is reasonable because the magnetic Reynolds number of fluid metals and partially ionized fluids commonly used in industrial applications is very small [17].

The vector form of governing equations of conservation of mass, momentum, energy, concentration of nanofluid are given by the following [6]:

$$\nabla \cdot \bar{U} = 0 \tag{1}$$

$$\rho_{nf}\left(\frac{\partial \bar{U}}{\partial t}\right) = -\nabla p + \mu_{nf}\nabla^2 \bar{U} + \bar{J} \times \bar{B} + gb \tag{2}$$

$$\left(\rho C_p\right)_{nf}\left(\frac{\partial T}{\partial t}\right) = -\nabla \cdot q \tag{3}$$

$$\frac{\partial C}{\partial t} = -\nabla \cdot j \tag{4}$$

where $\bar{U} = (u, v, w)$ is the velocity vector, ∇p is the pressure gradient, $\bar{B}$ is the magnetic field vector, b is the body forces, $q = -\kappa_{nf}\nabla T$ is the heat flux, $j = -D\nabla C$ is the mass flux and $\bar{J} = \sigma_{nf}\left(\bar{E} + \bar{U} \times \bar{B}\right)$ is the current density vector. Based on the above assumptions, the boundary layer equations of nanofluid flow, heat and mass transfer past an exponentially accelerated inclined plate are given by [6]:
Momentum Equation:

$$\begin{aligned}\rho_{nf}\left(\frac{\partial u'}{\partial t'}\right) &= \mu_{nf}\left(1+\frac{1}{\gamma}\right)\left(\frac{\partial^2 u'}{\partial y'^2}\right) - \sigma_{nf}B_0{}^2 u' + \left(\rho\beta\right)_{nf} g\left(T' - T'_\infty\right)(\cos\alpha) \\ &+ \left(\rho\beta^*\right)_{nf} g\left(T' - T'_\infty\right)(\cos\alpha) - \frac{\mu_{nf}u'}{K'}\end{aligned} \tag{5}$$

Energy Equation:

$$\frac{\partial T'}{\partial t'} = \frac{\kappa_{nf}}{\left(\rho C_p\right)_{nf}}\left(\frac{\partial^2 T'}{\partial y'^2}\right) - \frac{Q_o}{\left(\rho C_p\right)_{nf}}\left(T' - T'_\infty\right) - \frac{1}{\left(\rho C_p\right)_{nf}}\left(\frac{\partial q_r}{\partial y'}\right) \tag{6}$$

Species Diffusion Equation:

$$\frac{\partial C'}{\partial t'} = D_B\frac{\partial^2 C'}{\partial y'^2} - K'_r\left(C' - C'_\infty\right) + \frac{D_m k_T}{T_m}\left(\frac{\partial^2 T'}{\partial y'^2}\right) \tag{7}$$

For nanofluids, the expressions of density $\left(\rho_{nf}\right)$, thermal expansion coefficient $\left(\left(\rho\beta\right)_{nf}\right)$ and heat capacitance $\left(\left(\rho C_p\right)_{nf}\right)$ are given by

$$\left.\begin{aligned}&\rho_{nf} = (1-\varphi)\rho_f + \varphi\rho_s,\ \left(\rho\beta\right)_{nf} = (1-\varphi)\left(\rho\beta\right)_f + \varphi\left(\rho\beta\right)_s, \\ &\left(\rho\beta^*\right)_{nf} = (1-\varphi)\left(\rho\beta^*\right)_f + \varphi\left(\rho\beta^*\right)_s,\ \left(\rho C_p\right)_{nf} = (1-\varphi)\left(\rho C_p\right)_f + \varphi\left(\rho C_p\right)_s\end{aligned}\right\} \tag{8}$$

The effective thermal conductivity of the nanofluid according to the Hamilton and Crosser [18] model is given by

$$\kappa_{nf} = \kappa_f\left[\frac{\kappa_s + 2\kappa_f - 2\varphi\left(\kappa_f - \kappa_s\right)}{\kappa_s + 2\kappa_f + 2\varphi\left(\kappa_f - \kappa_s\right)}\right],\ \mu_{nf} = \frac{\mu_f}{(1-\varphi)^{2.5}} \tag{9}$$

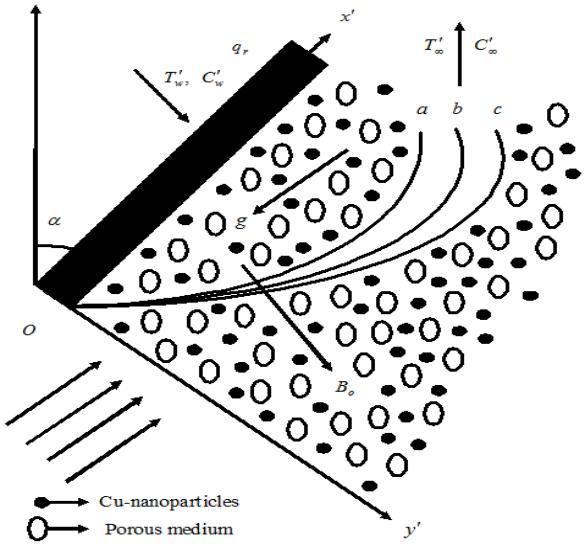

Fig. 1. Geometry of the problem: a - momentum boundary layer, b - thermal boundary layer, c - concentration boundary layer

The effective electrical conductivity of the nanofluid according to the Hamilton and Crosser [18] model is given by

$$\sigma_{nf} = \sigma_f \left[1 + \frac{3(\sigma - 1)\varphi}{\sigma + 2 - (\sigma - 1)\varphi} \right], \sigma = \frac{\sigma_s}{\sigma_f} \tag{10}$$

Table 1. Thermo physical properties

Physical properties	Water (base fluid)	*Cu* (Copper)
C_p (J/kg·K)	4179	385
ρ (kg/m^3)	997.1	8933
κ (W/m·K)	0.613	400
$\alpha \times 10^{-5}$ (1/K)	21	1.67

The thermo-physical properties of the pure fluid (water) and copper, which were used for code validation, are given in Table 1. Subject to the boundary conditions

$$\begin{aligned} t' \le 0 &: \left\{ u'(y', t') = 0,\ T'(y', t') = T'_\infty,\ C'(y', t') = C'_\infty \ \text{ for all } y' \right. \\ t' > 0 &: \left\{ \begin{array}{l} u'(y', t') = U_o \exp(a't'),\ T'(y', t') = T'_\infty + \dfrac{(T'_w - T'_\infty)U_o^2 t'}{\nu}, \\ C'(y', t') = C'_\infty + \dfrac{(C'_w - C'_\infty)U_o^2 t'}{\nu} \ \text{ at } \ y' = 0 \\ u'(y', t') = 0,\ T'(y', t') \to T'_\infty,\ C'(y', t') \to C'_\infty \ \text{ as } \ y' \to \infty \end{array} \right. \end{aligned} \tag{11}$$

For optically dense fluids, in addition to emission, there is self-absorption and the absorption coefficient usually depends on the wavelength and is large. Therefore, we can use the Rosseland approximation to obtain the radiation vector. Thermal radiation is supposed to occur in the form of a unidirectional flux in the y'-direction, i.e., q_r (transverse to the vertical surface). By using the Rosseland approximation [19], the radiative heat flux q_r is given by:

$$q_r = -4a^*\sigma\left(T_\infty'^4 - T'^4\right) \tag{12}$$

It should be noted that by using the Roseland's approximation, the present analysis is limited to optically thick fluids. If temperature differences within the flow are sufficiently small, then equation (12) can be linearized by expanding T'^4 in the Taylor series about T_∞' which after neglecting higher order terms takes the form:

$$T'^4 \cong T_\infty'^4 + 4\left(T' - T_\infty'\right)T_\infty'^3 = 4T'T_\infty'^3 - 3T_\infty'^4 \tag{13}$$

Using Eqs. (12) and (13) in the last term of Eq. (6), we obtain

$$\frac{\partial q_r}{\partial y'} = -16a^*\sigma^*T_\infty'^3\left(T' - T_\infty'\right) \tag{14}$$

Introducing (12) in the Eq. (6), the energy equation becomes

$$\frac{\partial T'}{\partial t'} = \frac{\kappa_{nf}}{\left(\rho C_p\right)_{nf}}\left(\frac{\partial^2 T'}{\partial y'^2}\right) - \frac{Q_o}{\left(\rho C_p\right)_{nf}}\left(T' - T_\infty'\right) - \frac{16a^*\sigma^*T_\infty'^3\left(T' - T_\infty'\right)}{\left(\rho C_p\right)_{nf}} \tag{15}$$

On introducing the following non-dimensional quantities

$$\left.\begin{aligned}
&u = \frac{u'}{U_o}, y = \frac{y'U_o}{\nu_f}, t = \frac{t'U_o^2}{\nu_f}, \theta = \frac{T' - T_\infty'}{T_w' - T_\infty'}, C = \frac{C' - C_\infty'}{C_w' - C_\infty'}, K = \frac{K'U_o^2}{\nu_f^2},\\
&M = \frac{\sigma_f\nu_f B_o^2}{\rho_f U_o^2}, a = \frac{\nu_f a'}{U_0^2}, \mathrm{Pr} = \frac{\left(\rho C_p\right)_f\nu_f}{\kappa_f}, Gr = \frac{\nu_f g\beta_f\left(T_w' - T_\infty'\right)}{U_o^3},\\
&R = \frac{16a^*\nu_f^2\sigma^*T_\infty'^3}{\kappa_f U_o^2}, Sc = \frac{\nu_f}{D_B}, Kr = \frac{K_r'\nu_f}{U_o^2}, S = \frac{Q_o\nu_f}{\left(\rho C_p\right)_f U_o^2},\\
&Gc = \frac{\nu_f g\beta_f^*\left(C_w' - C_\infty'\right)}{U_o^3}, Sr = \frac{D_m k_T\left(T_w' - T_\infty'\right)}{\nu T_m\left(C_w' - C_\infty'\right)}
\end{aligned}\right\} \tag{16}$$

then Eqs. (5), (7) and (15) transform to the following non-dimensional forms

$$\frac{\partial u}{\partial t} = L_1\left(1+\frac{1}{\gamma}\right)\frac{\partial^2 u}{\partial y^2} + L_2 Gr\left(\cos\alpha\right)\theta + L_3 Gc\left(\cos\alpha\right)C - L_4\left(M+\frac{1}{K}\right)u \tag{17}$$

$$\frac{\partial \theta}{\partial t} = L_5\frac{\partial^2 \theta}{\partial y^2} - L_6\theta \tag{18}$$

$$\frac{\partial C}{\partial t} = \frac{1}{Sc}\frac{\partial^2 C}{\partial y^2} - KrC + Sr\left(\frac{\partial^2 \theta}{\partial y^2}\right) \tag{19}$$

Where $x_1 = (1-\varphi) + \varphi\left(\frac{\rho_s}{\rho_f}\right)$, $x_2 = (1-\varphi) + \varphi\left(\frac{(\rho\beta)_s}{(\rho\beta)_f}\right)$,

$x_3 = (1-\varphi) + \varphi\left(\frac{(\rho\beta^*)_s}{(\rho\beta^*)_f}\right)$, $x_4 = \left[1 + \frac{3(\sigma-1)\varphi}{\sigma+2-(\sigma-1)\varphi}\right]$,

$x_5 = (1-\varphi) + \varphi\left(\frac{(\rho C_p)_s}{(\rho C_p)_f}\right)$, $x_6 = \frac{\kappa_{nf}}{\kappa_f} = \left[\frac{(1+2\varphi)+(2-2\varphi)\left(\frac{\kappa_f}{\kappa_s}\right)}{(1-2\varphi)+(2+2\varphi)\left(\frac{\kappa_f}{\kappa_s}\right)}\right]$,

$L_1 = \frac{1}{(1-\varphi)^{2.5}x_1}$, $L_2 = \frac{x_2}{x_1}$, $L_3 = \frac{x_3}{x_1}$, $L_4 = \frac{x_4}{x_1}$, $L_5 = \frac{1}{x_5\,\mathrm{Pr}}(x_6 + R)$, $L_6 = \frac{S}{x_5}$

The corresponding boundary conditions (11) in non-dimensional forms are

$$\begin{aligned} t \le 0: &\quad u = 0,\ \theta = 0,\ C = 0 \ \text{ for all } y \\ t > 0: &\quad \left\{\begin{aligned} &u = \exp(at),\ \theta = t,\ C = t \ \text{ at } y = 0 \\ &u \to 0,\ \theta \to 0,\ C \to 0 \quad \text{as } y \to \infty \end{aligned}\right\} \end{aligned} \tag{20}$$

The skin-friction at the plate, which is the non-dimensional form, is given by

$$Cf = \left(1+\frac{1}{\gamma}\right)\frac{\left(\frac{\partial u'}{\partial y'}\right)_{y'=0}}{\rho_f U_o \nu_f} = \left(1+\frac{1}{\gamma}\right)\frac{1}{(1-\varphi)^{2.5}}\left(\frac{\partial u}{\partial y}\right)_{y=0} \tag{21}$$

The rate of heat transfer coefficient, which is the non-dimensional form in terms of the Nusselt number (*Nu*), is given by

$$Nu = -\left(\frac{x'}{T'_w - T'_\infty}\right)\left(\frac{\partial T'}{\partial y'}\right)_{y'=0} \Rightarrow Nu\,\mathrm{Re}_x^{-1} = -\left(\frac{\kappa_{nf}}{\kappa_f}\right)\left(\frac{\partial \theta}{\partial y}\right)_{y=0} \tag{22}$$

The rate of mass transfer coefficient, which is the non-dimensional form in terms of the Sherwood number (*Sh*), is given by

$$Sh = -\left(\frac{x'}{C'_w - C'_\infty}\right)\left(\frac{\partial C'}{\partial y'}\right)_{y'=0} \Rightarrow Sh\,\mathrm{Re}_x^{-1} = -\left(\frac{\partial C}{\partial y}\right)_{y=0} \tag{23}$$

where $\mathrm{Re} = \dfrac{U_o x'}{\nu_f}$ is the local Reynolds number.

3. Mathematical explanations through finite difference technique

The non-linear momentum, energy and concentration equations given in equations (17), (18) and (19), are solved under the appropriate initial and boundary conditions (20) by the implicit finite difference method [20]. The transport equations (17), (18) and (19) at the grid point (i, j) are expressed in differences form using Taylor's expansion

$$\left(\frac{u_i^{j+1} - u_i^j}{\Delta t}\right) = L_1\left(1 + \frac{1}{\gamma}\right)\left(\frac{u_{i+1}^j - 2u_i^j + u_{i-1}^j}{(\Delta y)^2}\right) + L_2(Gr)(\cos\alpha)\theta_i^j$$
$$+ L_3(Gc)(\cos\alpha)C_i^j - L_4\left(M + \frac{1}{K}\right)u_i^j \tag{24}$$

$$\left(\frac{\theta_i^{j+1} - \theta_i^j}{\Delta t}\right) = L_5\left(\frac{\theta_{i+1}^j - 2\theta_i^j + \theta_{i-1}^j}{(\Delta y)^2}\right) - L_6\theta_i^j \tag{25}$$

$$\left(\frac{C_i^{j+1} - C_i^j}{\Delta t}\right) = \frac{1}{Sc}\left(\frac{C_{i+1}^j - 2C_i^j + C_{i-1}^j}{(\Delta y)^2}\right) - KrC_i^j + Sr\left(\frac{\theta_{i+1}^j - 2\theta_i^j + \theta_{i-1}^j}{(\Delta y)^2}\right) \tag{26}$$

Thus the values of u, θ and C at grid point $t = 0$ are known; hence the temperature field has been solved at time $t_{i+1} = t_i + \Delta t$ using the known values of the previous time $t = t_i$ for all $i = 1, 2, ..., N-1$. Then the velocity field is evaluated using the already known values of temperature and concentration fields obtained at $t_{i+1} = t_i + \Delta t$. These processes are repeated till the required solution of u, θ and C is gained at convergence criteria:

$$abs\left|(u,\ \theta,\ C)_{exact} - (u,\ \theta,\ C)_{numerical}\right| < 10^{-3} \tag{27}$$

4. Comparison for code validation

To discuss the validation code for the finite difference method, we compared the present numerical results with the published closed form solutions described by Pattnaik et al. [6] in the absence of *Cu*-nanoparticles, thermal diffusion and Casson fluid effects. This code validation is discussed and presented in Tables 2, 3 and 4. From these tables, we found that our numerical results are consistent with the exact results of Pattnaik et al. [6].

Table 2. Comparison of present skin-friction coefficient results (*Cf*) due to velocity profiles with the skin-friction coefficient results (τ) of Pattnaik et al. [6] in the absence of *Cu*-nanoparticles, thermal diffusion and Casson fluid effects

Gr	*M*	*Pr*	*Sc*	*R*	*S*	τ	*Cf*
10.0	1.00	0.71	0.60	4.00	2.00	1.2389	1.2296064578
15.0	1.00	0.71	0.60	4.00	2.00	1.6663	1.6554721057
10.0	**5.00**	0.71	0.60	4.00	2.00	0.9254	0.9155230178
10.0	1.00	**0.10**	0.60	4.00	2.00	1.1909	1.1898553015
10.0	1.00	0.71	**0.30**	4.00	2.00	1.1503	1.1432298633
10.0	1.00	0.71	0.60	**7.00**	2.00	1.3072	1.2966347826
10.0	1.00	0.71	0.60	4.00	**9.00**	1.4614	1.4523386111

Table 3. Comparison of present Nusselt number results due to concentration profiles with the Nusselt number results of Pattnaik et al. [6] in absence of *Cu*-nanoparticles, thermal diffusion and Casson fluid effects

R	*Pr*	*S*	*t*	Present Nusselt number results	Nusselt number results of Pattnaik et al. [6]
4.0	0.71	2.0	0.2	0.5118524618	0.5214
10.0	0.71	2.0	0.2	0.6788210455	0.6832
4.0	**0.50**	2.0	0.2	0.4766201897	0.4849
4.0	0.71	**7.0**	0.2	0.4533290173	0.4629
4.0	0.71	2.0	**0.5**	1.0186021869	1.0208

Table 4. Comparison of present Sherwood number results due to concentration profiles with the Sherwood number results of Pattnaik et al. [6] in absence of *Cu*-nanoparticles, thermal diffusion and Casson fluid effects

Sc	*Kr*	*t*	Present Sherwood number results	Sherwood number results of Pattnaik et al. [6]
0.60	0.20	0.40	0.5594262189	0.5674
0.30	0.20	0.40	1.2566084877	1.2688
0.60	**2.00**	0.40	0.6755264893	0.6896
0.60	0.20	**0.80**	0.8199630215	0.8228

5. Results and discussions

Unsteady hydromagnetic uni-directional radiative flow of a Casson fluid along a vertical inclined porous plate including the effects of chemical reaction and *Cu*-nanoparticles is investigated. The numerical results showing the impact of pertinent flow parameters, such as the Casson fluid parameter γ, magnetic field parameter M, angle of inclination parameter α, thermal diffusion parameter Sr, Schmidt number Sc, Prandtl number Pr, thermal radiation parameter R, heat source parameter S, chemical reaction parameter Kr and time t on the velocity, temperature, concentration fields are depicted in 2 to 14. Figure 2 presents the velocity profiles for various values of magnetic field parameter M for the *Cu*-nanoparticles and regular fluid. From this graphs, it is obvious that the nanofluid velocity of the fluid decelerates with an increase in the strength of the magnetic field.

The effects of a transverse magnetic field on an electrically, conducting fluid give rise to a resistive-type force called the Lorentz force. This force has the tendency to slow down the motion of the fluid in the boundary layer. These results are quantitatively agree with the expectations, since the magnetic field exerts retarding force on natural convection flow.

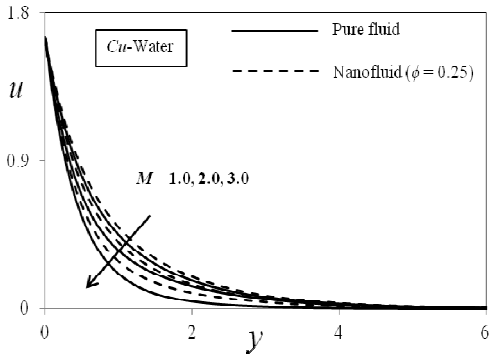

Fig. 2. M results on u

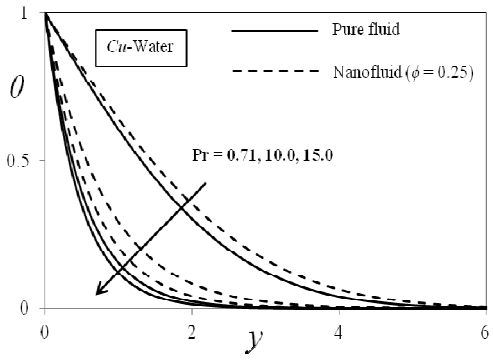

Fig. 3. Pr result on θ

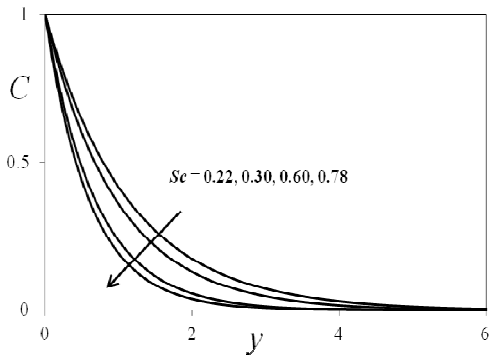

Fig. 4. Sc effect on C

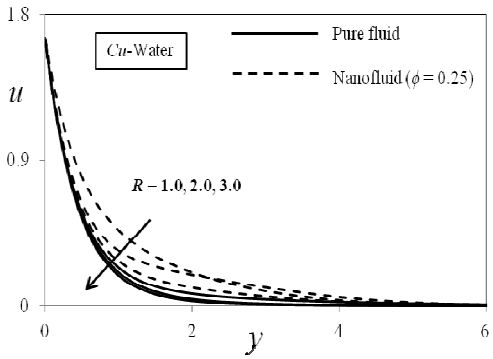

Fig. 5. R effect on u

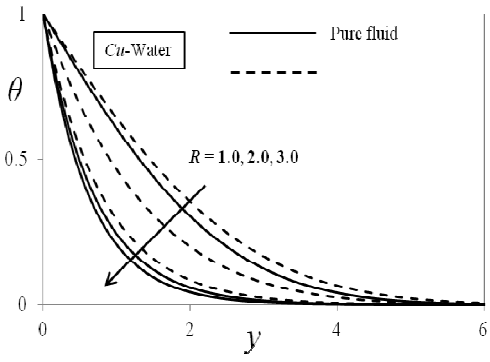

Fig. 6. *R* effect on θ

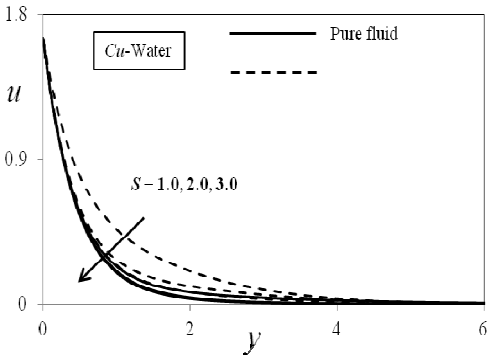

Fig. 7. *S* effect on *u*

Figure 3 illustrates the numerical results of temperature profiles for different values of Prandtl number Pr in the presence of foreign species such as Mercury (Pr = 0.025), Air (Pr = 0.71), Water (Pr = 7.00) and Water at 4°C (Pr = 11.40). The Prandtl number signifies the ratio of momentum diffusivity to thermal diffusivity. From this figure, it is observed that an increase in the Prandtl number results in a decrease of the thermal boundary layer thickness and, in general, lower average temperature within the boundary layer. Heat is able to diffuse away from the heated surface more rapidly for higher values of Pr as smaller values of Pr are equivalent to increasing the thermal conductivities. Hence, in the case of smaller Prandtl numbers, the boundary layer is thicker and the rate of heat transfer is reduced. From these figures, it is also observed that in the case of *Cu*-nanoparticles, thermal boundary layer is higher than that of regular base fluid. The effect of Schmidt number *Sc* for different heavier diffusing species such as *Sc* = 0.22 (hydrogen), *Sc* = 0.30 (helium), *Sc* = 0.60 (water vapour), *Sc* = 0.78 (ammonia) with respect to concentration are visualized in Figure 4. As Schmidt number *Sc* is a ratio of the viscous diffusion rate to the mass diffusion rate. Hence, with growth in Schmidt number *Sc* the concentration profiles declines.

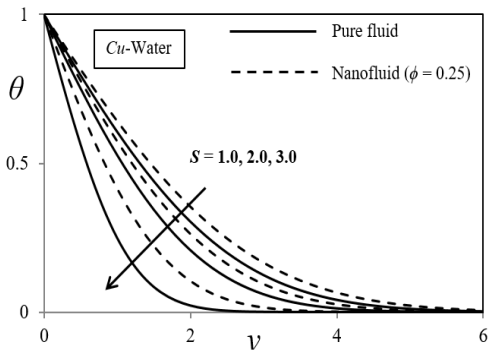

Fig. 8. *S* influence on θ

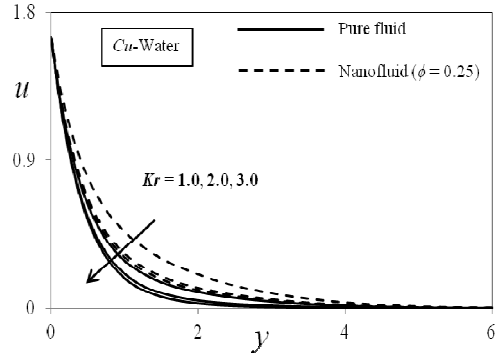

Fig. 9. *Kr* outcomes on *u*

For various values of thermal radiation parameter R, the velocity and temperature profiles are plotted in Figures 5 and 6. The thermal radiation parameter R defines the relative contribution of the conduction heat transfer to thermal radiation transfer The radiation parameter R defines the relative contribution of conduction heat transfer to thermal radiation transfer. It is obvious that an increase in the radiation parameter results in decreasing velocity and temperature within the boundary layer. Figures 7 and 8 have been plotted to find the variation of velocity and temperature profiles for different values of heat source parameter S by fixing other parameters. These figures clearly demonstrates that there is a decrease in velocity and temperature with an increase in S. The fact states that, when heat is absorbed, the buoyancy force decreases which retards the flow rate and thereby decreases the velocity and temperature profiles, explains this occurrence. Figures 9 and 10 display the effects of the chemical reaction parameter Kr on the velocity and concentration profiles. As expected, the presence of the chemical reaction influences the concentration profiles as well as the velocity profiles to a large extent. It should be mentioned here that the case study is a destructive chemical reaction.

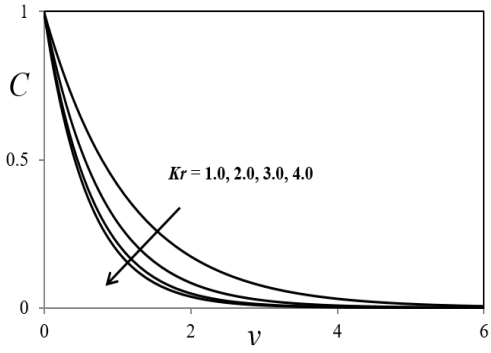

Fig. 10. Kr result on C

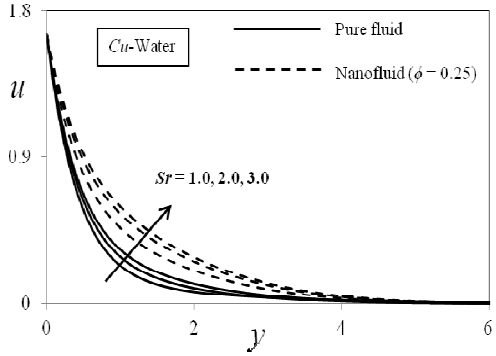

Fig. 11. Sr influence on u

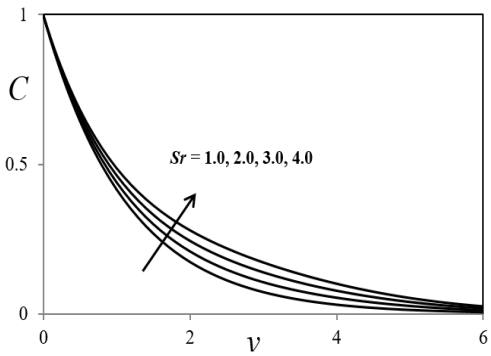

Fig. 12. Sr effect on C

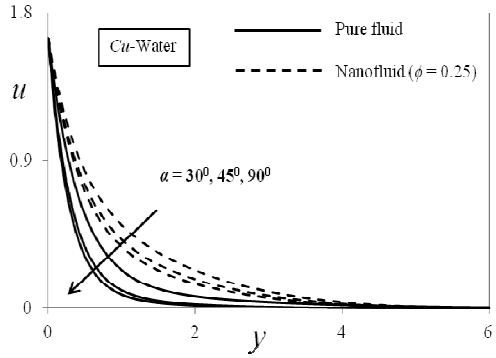

Fig. 13. α effect on u

In fact, as chemical reaction increases, the considerable reduction in the velocity profiles is predicted, and the presence of the peak indicates that the maximum

value of the velocity occurs in the body of the fluid close to the surface but not at the surface. Also, a rise in the chemical reaction parameter leads to the reduction in the concentration. It is obvious that the increase in the chemical reaction alters the concentration boundary layer thickness but not the momentum boundary layers.

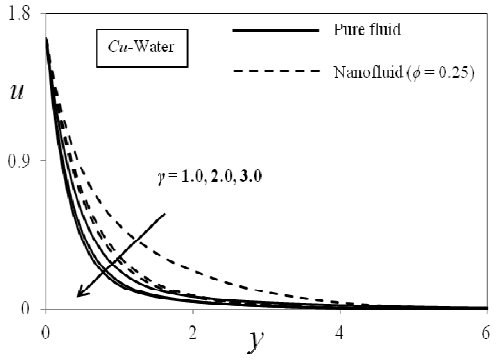

Fig. 14. γ influence on u

Figures 11 and 12 depict the velocity and concentration profiles for different values of the Soret number *Sr*. The Soret number *Sr* defines the effect of the temperature gradients inducing significant mass diffusion effects. It is noticed that a rise in the Soret number *Sr* results in the augment of the velocity and concentration within the boundary layer. In Figure 13, the effect of an inclination (α) on velocity profiles are shown. Observations indicate a decrease in velocity profiles due to the increase in α. It is further mentioned that an increase in the angle of inclination reduces the velocity at all points, as the forcing forces are depleted due to the factor $cos\alpha$. Figure 14, the effect of the Casson fluid parameter, is shown on the nanofluid velocity profiles. In Figure 14, it can be seen that by increasing γ, the velocity has decreased. Physically, an increase in γ causes an increase in fluid viscosity, so it is obvious that the higher viscosity results in lower velocity.

6. Conclusions

The purpose of this study was to obtain numerical solutions for unsteady free convective Casson fluid flow past a vertical plate in the presence of a transverse uniform magnetic field and *Cu*-nanoparticles. The effects of the pertinent parameters on velocity, concentration and temperature profiles are presented graphically. The most important concluding remarks can be summarized as follows:

i. The velocity profiles are increasing under the increasing of thermal diffusion parameter *Sr*. The velocity profiles are decreasing under the increasing of Casson fluid parameter γ, magnetic field parameter *M*, angle of inclination parameter α, thermal radiation parameter *R*, heat source parameter *S* and Chemical reaction parameter *Kr*.

ii. The temperature profiles are decreasing with the increasing of Prandtl number Pr, thermal radiation parameter *R* and heat source parameter *S*.
iii. The concentration profiles are increasing with increasing values of Thermal diffusion parameter *Sr* and decreasing with increasing of Schmidt number *Sc* and chemical reaction parameter *Kr*.
iv. This study exactly agrees with the finding of previous results of Pattnaik et al. [6] in absence of *Cu*-nanoparticles, Casson fluid and thermal diffusion effects.

References

[1] Anbuchezhian, N., Srinivasan, K., Chandrasekaran, K., & Kandasamy, R. (2012). Thermophoresis and Brownian motion effects on boundary layer flow of nanofluid in presence of thermal stratification due to solar energy. *Applied Mathematics and Mechanics*, *33*, 765-780.

[2] Hayat, T., Qayyum, S., Imtiaz, M., & Alsaedi, A. (2016). Comparative study of silver and copper water nanofluids with mixed convection and nonlinear thermal radiation. *International Journal of Heat and Transfer*, *102*, 723-732.

[3] Hayat, T., Qayyum, S., Alsaedi, A., & Shafiq, A. (2016). Inclined magnetic field and heat source/sink aspects in flow of nanofluid with nonlinear thermal radiation. *International Journal of Heat and Transfer*, *103*, 99-107.

[4] Akdag, U., Akcay, S., & Demiral, D. (2014). Heat transfer enhancement with laminar pulsating nanofluid flow in a wavy channel. *International Journal of Communications in Heat Mass Transfer*, *59*, 17-23.

[5] Hayat, T., Shafiq, A., Imtiaz, M., & Alsaedi, A. (2016). Impact of melting phenomenon in the Falkner-Skan wedge flow of second grade nanofluid: a revised model. *Journal of Molecular Liquids*, *215*, 664-670.

[6] Pattnaik, J.R., Dash, G.C., & Singh, S. (2017). Radiation and mass transfer effects on MHD flow through porous medium past an exponentially accelerated inclined plate with variable temperature. *Ain Shams Engineering Journal*, *8*, 67-75.

[7] Krishna Prasad, D.V.V., Krishna Chaitanya, G.S., & Srinivasa Raju, R. (2019). Double diffusive effects on mixed convection Casson fluid flow past a wavy inclined plate in presence of Darcian porous medium. *Results in Engineering Journal*, *3*, 100019.

[8] Srinivasa Raju, R., Jithender Reddy, G., Anil Kumar, M., & Rama Subba Reddy Gorla, (2019). Jeffrey Fluid Impact on MHD free convective flow past a vertically inclined plate with transfer effects: EFGM solutions. *International Journal of Fluid Mechanics Research*, *46*(3), 239-260.

[9] Sarada, K., Malleswari, D., & Srinivasa Raju, R. (2019). Heat and mass transfer effects on chemical reacting fluid flow past, An exponentially accelerated vertical plate. *AIP Conference Proceedings Journal*, *2142*, 170005-1-170005-5.

[10] Jitthender Reddy, G., Srinivasa Raju, R., & Anand Rao, J. (2018). Influence of viscous dissipation on unsteady MHD natural convective flow of Casson fluid over an oscillating vertical plate via FEM. *Ain Shams Engineering Journal*, *9*, 1907-1915.

[11] Srinivasa Raju, R. (2018). Unsteady MHD boundary layer flow of Casson fluid over an inclined surface embedded in a porous medium with thermal radiation and chemical reaction. *Journal of Nano Fluids*, *7*(4), 694-703.

[12] Rafique, K., Anwar, M.I., Misiran, M., Khan, I., Seikh, A.H., Sherif, E.S.M., & Nisar, K.S. (2019). Brownian motion and thermophoretic diffusion effects on micropolar type nanofluid flow with Soret and Dufour impacts over an inclined sheet: Keller-box simulations. *Energies*, *12*(21), 4191.

[13] Rafique, K., Anwar, M.I., Misiran, M., Khan, I., Alharbi, S.O., Thounthong, P., & Nisar, K.S. (2019). Numerical solution of Casson nanofluid flow over a nonlinear inclined surface with Soret and Dufour effects by Keller-box method. *Frontiers in Physics*, *7*(139), DOI: 10.3389/fphy.

[14] Rafique, K., Anwar, M.I., Misiran, M., Khan, I., Alharbi, S.O., Thounthong, P., & Nisar, K.S. (2019). Keller-box analysis of Buongiorno model with Brownian and thermophoretic diffusion for Casson nanofluid over an inclined surface. *Symmetry*, *11*(11), 1370.

[15] Rafique, K., Anwar, M.I., Misiran, M., Khan, I., Seikh, A.H., Sherif, E.S.M., & Nisar, K.S. (2019). Numerical analysis with Keller-box scheme for stagnation point effect on flow of micro-polar nanofluid over an inclined surface. *Symmetry*, *11*(11), 1379.

[16] Anwar, M.I., Rafique, K., Misiran, M., & Shehzad, S.A. (2020). Numerical study of hydro-dynamic flow of a Casson nanomaterial past an inclined sheet under porous medium. *Heat Transfer-Asian Research*, 49, 307-334, https://doi.org/10.1002/htj.21614.

[17] Cramer, K.R., & Pai, S.I. (1973). *Magneto-fluid Dynamics for Engineers and Applied Physi-cists*. NY: McGraw Hill Book Company.

[18] Hamilton, R.L., & Crosser, O.K. (1962). Thermal conductivity of heterogeneous two component systems. *I and EC Fundamentals*, *1*(3), 187-191.

[19] Sparrow, E.M., & Cess, R.D. (1966). *Radiation Heat Transfer*. Belmont, Calif.: Brooks/Cole.

[20] Omeshwar Reddy, V., Neelima, A., & Thiagarajan, S. (2019). Finite difference solutions of MHD natural convective Rivlin-ericksen fluid flow past a vertically inclined porous plate in presence of thermal diffusion, diffusion thermo, heat and mass transfer effects. *International Journal of Applied Engineering Research*, *14*(3), 703-716.